Photo-induced phase transitions in ferroelectrics

Charles Paillard, Engin Torun, Ludger Wirtz, Laurent Bellaïche

Photo-induced phase transitions in ferroelectrics

Charles Paillard,[1,2] Engin Torun,[3] Ludger Wirtz,[3] Jorge Íñiguez,[4,3] and Laurent Bellaiche[1]

[1] *Department of Physics and Institute for Nanoscience and Engineering, University of Arkansas, Fayetteville, Arkansas 72701, USA*

[2] *Laboratoire Structures, Propriétés et Modélisation des Solides, CentraleSupélec, UMR CNRS 8580, Université Paris-Saclay, 91190 Gif-sur-Yvette, France**

[3] *Physics and Materials Science Research Unit, University of Luxembourg, 162a avenue de la Faïencerie, L-1511 Luxembourg, Luxembourg*

[4] *Materials Research and Technology Department, Luxembourg Institute of Science and Technology (LIST), Avenue des Hauts-Fourneaux 5, L-4362 Esch/Alzette, Luxembourg*

Ferroic materials naturally exhibit a rich number of functionalities, which often arise from thermally, chemically or mechanically induced symmetry breakings or phase transitions. Based on Density Functional Calculations, we demonstrate here that light can drive phase transitions as well in ferroelectric materials such as the perovskite oxides lead titanate and barium titanate. Phonon analysis and total energy calculations reveal that the polarization tends to vanish under illumination, to favor the emergence of non-polar phases, potentially antiferroelectric, and exhibiting a tilt of the oxygen octahedra. Strategies to tailor photo-induced phases based on phonon instabilities in the electronic ground state are also discussed.

Ferroelectric materials possess a spontaneous electric polarization that is switchable by electric fields. Active research in bandgap engineering [1] and unconventional photovoltaic mechanisms [2–4] have prompted perovskite oxide ferroelectrics as potential light absorbers to convert light into electric [5], mechanical [6–8] or chemical energy [9], or for optical memory writing [10] and non-destructive reading [11]. Numerous works focused on the photo-induced deformation of the unit cell without apparent symmetry breaking [8]. However, a recent experimental work hinted at possible structural phase transitions occurring in ferroelectric $BaTiO_3$ nanowires under illumination [12]. Using first-principles calculations, we show that photo-induced phase transitions are indeed possible in ferroelectrics such as barium and lead titanates. In both cases, transitions to non-polar phases are predicted. Furthermore, material engineering strategies based on competing lattice instabilities are suggested to tailor the critical concentration of photo-induced carriers at which the transition occurs, thus opening the way to a rational design of materials exhibiting specific properties under illumination.

ABO_3 perovskite oxides are versatile materials exhibiting a wide range of properties (magnetism, polar distortions, etc.). Their high symmetry reference structure (see Fig. 1) is cubic with the B cation enclosed in an octahedral cage of oxygens at the center, and the A cation at the edges of the cube. Simple atomic displacement patterns – e.g. as the octahedra tilts or electric dipoles sketched in Fig. 1 – make it possible to obtain various symmetry breakings and control the materials properties. For convenience, here we denote the most relevant of such distortions using a generalized and simplified Glazer notation [13] $\alpha\beta\gamma/u^{\alpha'}v^{\beta'}w^{\gamma'}$, which is introduced in the caption of Fig. 1.

Among perovskite oxides, barium titanate (BTO) and lead titanate (PTO) are prototypical ferroelectric materials. They exhibit a number of phases [14, 15] associated with lattice instabilities of the reference cubic phase [16]. The transitions between phases are commonly driven by temperature [14, 15], pressure [17–19] or static electric fields [20]. Here, we demonstrate that light can also act as a knob to control the crystal symmetry. Optical manipulation of ferroic materials has mainly focused on the transient manipulation of the ferroic order parameter, relying on non-thermalized photoexcited carriers [21] or strong anharmonic phonon couplings [22]. In contrast, we presently describe the emergence of new phases caused by modified lattice instabilities in the presence of thermalized photo-excited carriers, *i.e.* the electrons lying at the bottom of the conduction band (CB) and the equal number of holes sitting at the top of the valence band (VB) of a semiconductor during illumination. To this end, we used *ab-initio* calculations, detailed in the next section, before examining the cases of barium and lead titanate respectively. Finally, we discuss the origin of this phenomenon and test design strategies for the engineering of photo-induced phase transitions in ferroelectrics.

We performed Density Functional Theory (DFT) calculations using the Abinit package software [23], with the Projector Augmented Wave (PAW) method [24, 25]. We employ a $2 \times 2 \times 2$ supercell (with respect to the 5-atom pseudo-cubic perovskite cell) containing 40 atoms. The k-point mesh used was a Γ-centered $8 \times 8 \times 8$ grid; the plane-wave cut-off was 35 Ha. A Fermi-Dirac distribution with 0.1 eV smearing was used to populate the electronic states. The electronic density was considered converged when the difference in the calculated forces between two Self-Consistent Field (SCF) steps was smaller than 10^{-8} Ha.Bohr^{-1}. The structural relaxation was

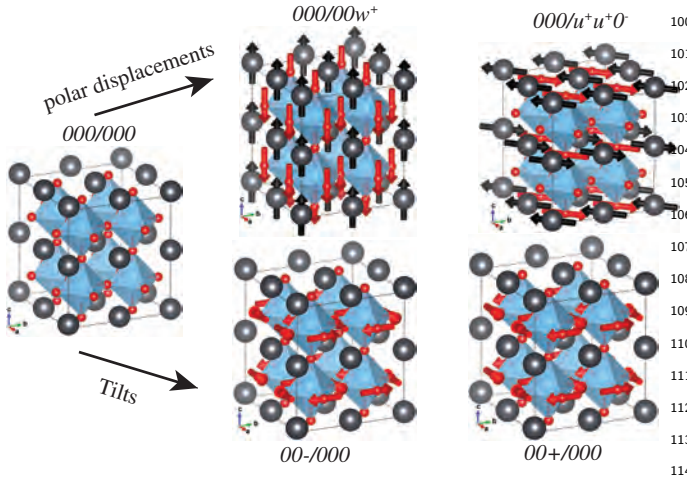

FIG. 1. Sketch of a $2\times2\times2$ supercell in the paraelectric cubic reference structure 000/000. A and B cations are in black and blue, oxygens in red. The symmetry of a phase is denoted by *(i)* its oxygen octahedra tilt pattern $\alpha\beta\gamma$, where α, β and γ are either 0 (no tilt), "+" (in-phase tilt) or "−" (antiphase tilt) and represent whether the oxygen octahedra tilts around the first, second and third pseudocubic axis, respectively. Similarly, we denote the electric dipole pattern using a Glazer-like notation $u^{\alpha'}v^{\beta'}w^{\gamma'}$, in which u, v, w represent the magnitude of the dipole inside the perovskite 5-atom cell, and α', β' and γ' describes whether dipole vectors $[uvw]$ are aligned parallel ("+") or antiparallel ("−") when moving by one perovskite 5-atom cell along the first, second and third pseudocubic direction. Typical polar ($000/00w^+$), antipolar ($000/u^+u^+0^-$), in-phase ($00c^+/000$) and antiphase tilt ($00c^-/000$) displacement patterns are depicted using arrows.

stopped when all the forces on the atoms were smaller than 5×10^{-7} Ha.Bohr^{-1} and all components of the stress tensor smaller than 0.1 MPa. BTO was described using the PBESol [26] exchange-correlation functional, while the Local Density Approximation [27, 28] was employed to treat PTO. Photo-excited thermalized carriers are mimicked using Fermi-Dirac distribution with two quasi-Fermi levels μ_e and μ_h, as commonly used to describe photovoltaic effects in, for instance, $p-n$ junctions [29]. As a result, during our DFT calculations, the density is self-consistently converged under the constraint of having $n_e = n_{ph}$ (and $n_h = n_{ph}$) electrons (holes) in the CB (VB). In other words, at each Self-Consistent Field (SCF) iteration, the following system of equations

$$n_h = \sum_{i\leq N_v}\sum_{\boldsymbol{k},\sigma} w_{\boldsymbol{k}}[1-f(\varepsilon_{i\boldsymbol{k},\sigma},\mu_h)], \quad (1)$$

$$n_e = \sum_{i> N_v}\sum_{\boldsymbol{k},\sigma} w_{\boldsymbol{k}} f(\varepsilon_{i\boldsymbol{k},\sigma},\mu_e), \quad (2)$$

is solved for μ_e and μ_h using a bisection algorithm. In the above equation, $w_{\boldsymbol{k}}$ is the weight of k-point $\boldsymbol{k}$, $f(\varepsilon_{i\boldsymbol{k}},\mu)$ is the occupation number (Fermi-Dirac distribution) of state with eigenvalue $\varepsilon_{i\boldsymbol{k}}$; σ denotes the spin. N_v is the index of the highest valence band. We assume that there is no closing of the gap during our constrained DFT calculations, which is in practice observed for the concentrations of photo-excited carrier pairs n_{ph} considered in this work.

Note that all structures considered in this work were geometrically relaxed under the photo-excitation constraint mentioned above. The criteria for convergence of the structural degrees of freedom are set to be the same as in electronic ground state calculations.

Phonon calculations using the Phonopy package [30] were performed in the dark and under excitation on the cubic perovskite oxides using a $2\times2\times2$ supercell after the system was structurally relaxed. No analytic correction, and thus no LO-TO splitting was considered, as the required Born effective charges cannot be calculated in photo-excited cases.

We first calculated the phonon band structure of cubic BTO in Figs. (2.a-d) for different concentrations of photoexcited carriers n_{ph}. In the dark ($n_{ph}=0$ e/f.u., Fig. (2.a)), the phonon dispersion exhibits imaginary (negative in the figure) frequency modes characteristic of lattice instabilities. The main instability, at Γ, is responsible for the emergence of the polar order in BTO [16], which goes from a high temperature cubic 000/000 structure to a ferroelectric tetragonal $000/00w^+$ phase below ∼393 K, then to an orthorhombic structure $000/0v^+v^+$ below ∼280-270 K and finally to a rhombohedral $000/u^+u^+u^+$ phase below ∼183 K [14]. Upon increasing the number of photo-excited carrier pairs to $n_{ph}=0.05$ e/f.u. (in Fig. (2.b)), the frequencies of unstable modes along the $X-M-\Gamma$ path get closer to real (positive) values, the ferroelectric soft optical mode at Γ becoming less unstable. Furthermore, for $n_{ph}\geq0.1$ e/f.u. (Figs. (2.c-d)) the cubic phase no longer exhibits unstable phonon modes and is *dynamically stable*!

We calculated the energy (see Fig. (3.a)) of the four phases naturally occurring in bulk BTO, 000/000 (green squares), $000/00w^+$ (blue diamonds), $000/0v^+v^+$ (violet triangles) and $000/u^+u^+u^+$ (ground state at 0 K in dark conditions, black dashed baseline). The rhombohedral phase has the lowest energy for low concentrations of photo-excited carriers (up to ≈0.0375 e/f.u.), while the tetragonal phase is slightly more stable at intermediate concentrations ($n_{ph}\approx0.0375-0.1$ e/f.u.). When the cubic phase is dynamically stable ($n_{ph}>0.1$ e/f.u.), we find accordingly that 000/000 is the lowest-energy structure, which is confirmed by the disappearance of polar atomic displacements and the cell shape distortions of all considered phases (see Supplementary Material [31]). The predicted transition towards the 000/000 phase is consistent with the experimental observation, in BTO, of a downward shift of the Curie temperature under illumination [32]. Besides, the flattening of the energy landscape around 0.03 e/f.u. ($\approx5\times10^{20}$ e.cm^{-3}) may be accompanied by a monoclinic phase transition (see Supplemental

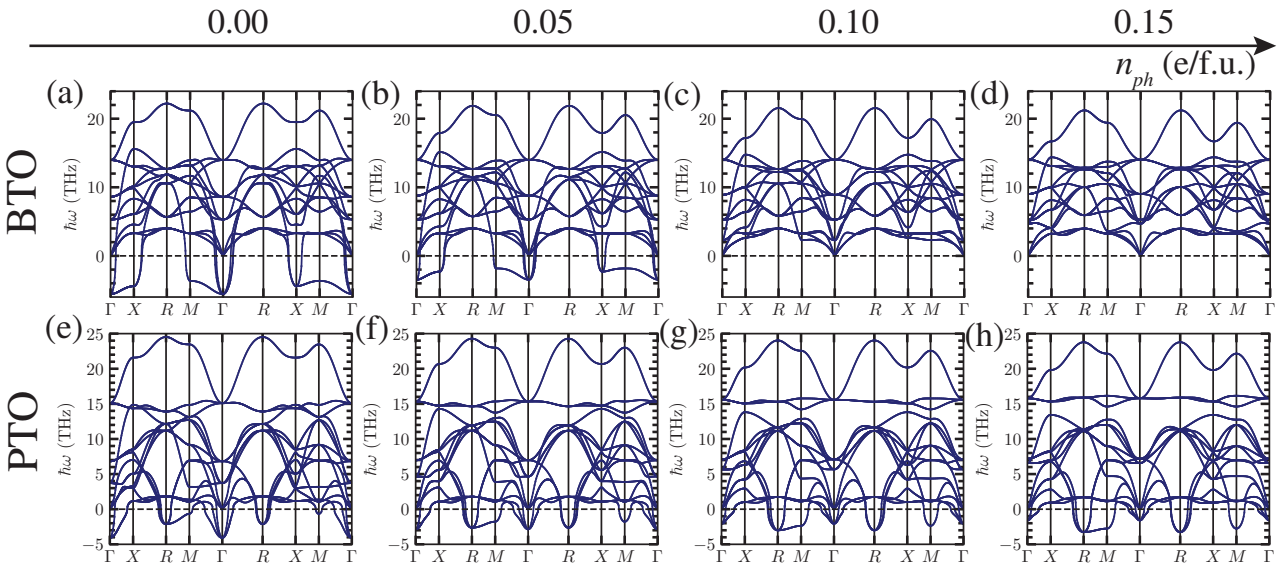

FIG. 2. (a-d) Phonon band structure in paraelectric cubic BTO and (e-h) PTO for different concentrations of photoexcited carrier pairs $n_{ph} = 0.00$ e/f.u. (a & e), $n_{ph} = 0.05$ e/f.u. (b & f), $n_{ph} = 0.10$ e/f.u. (c & g) and $n_{ph} = 0.15$ e/f.u. (d & h). The polar Γ dominant instability in BTO becomes stabilized (*i.e.* positive and real frequency) for $n_{ph} \geq 0.10$ e/f.u., as shown in (c) and (d). In PTO, the polar instability at Γ is replaced by a non-polar tilted instability at M and R.

Material [31]). We note that such a critical concentration would match recent observations of a monoclinic phase in BTO nanowires under illumination [12, 33].

PTO exhibits a single transition from the non-polar cubic 000/000 phase to the ferroelectric tetragonal $000/00w^+$ structure below 765 K [15]. The phonon dispersion of the cubic phase for $n_{ph} = 0$ e/f.u. (Fig. (2.e)) exhibits one main polar instability at Γ, but also unstable modes at the R and M points associated with octahedra tilting 00− and 00+, respectively. The strength of the polar instability at Γ decreases with increasing the number of photo-excited carriers (see Figs. (2.e-h)) as in BTO. However, it never totally disappears, indicating that ferroelectricity in PTO is more robust against photocarrier generation. In contrast, the strengths of the tilting instabilities at R and M are slightly enhanced, and they become dominant for $n_{ph} \geq 0.1$ (Figs. (2.g-h)), suggesting a transition from a polar to a non-polar structure with oxygen tilts under illumination.

Hence, we compute the energies of several prototypical phases upon illumination, as shown in Fig. (3.b). The ferroelectric $000/00w^+$ phase, which is the ground state in dark conditions, is the black dashed baseline, while the cubic phase is plotted as green squares. We also plot a rhombohedral polar $---/u^+u^+u^+$ structure (navy circles) and its non-polar counterpart, $a---/000$ (navy diamonds). We consider as well an orthorhombic phase (violet triangles) with the $--0/u^-\bar{u}^-0^-$ antipolar displacement pattern [34]. A $00c^-/000$ non-polar tetragonal phase is also calculated (gold triangles). According to Fig. (3.b), the ferroelectric $000/00w^+$ phase is the most stable up to $n_{ph} \approx 0.125$ e/f.u., the non-polar phase with tilts becoming dominant beyond that point. Overall, the antipolar $--0/u^-\bar{u}^-0^-$ phase is slightly more favorable (by 0.2-0.3 meV/f.u.) than the $---/000$ phase for $n_{ph} \geq 0.125$ e/f.u. Because of this small energy difference, it is impossible to predict with certainty the symmetry of PTO at large concentrations of photo-excited carriers, and we can only reckon that this should be a phase with oxygen tilts.

Unlike BTO, the polar atomic distortion in the $000/00w^+$ phase remains rather large under photoexcitation (see Supplementary Material [31]). Moreover, both the antipolar displacement (for the $--0/u^-\bar{u}^-0^-$ phase) and the tilt angle (for $---/000$ and $--0/u^-\bar{u}^-0^-$) increase with n_{ph}. In contrast, the polar displacements of the $---/u^+u^+u^+$ phase disappear with increasing n_{ph}, and it thus collapses into the $---/000$ phase, confirming that tilts and polarization are competing order parameters in PTO [35, 36], illumination tipping the balance towards the former.

Furthermore, calculations of minimum energy transition paths between phases (see Supplementary Material [31]) show that $--0/u^-\bar{u}^-0^-$ and $---/000$ are unstable in the dark; however, the $000/00w^+$ phase remains metastable under illumination, drawing the picture of a first-order light-induced transition in PTO.

The large concentration of 0.125 e/f.u. needed to destabilize the $000/00w^+$ phase in PTO is potentially outside the reach of experiments, and certainly not desirable for applications. We can try to improve this situation by mixing PTO with an antiferrodistortive

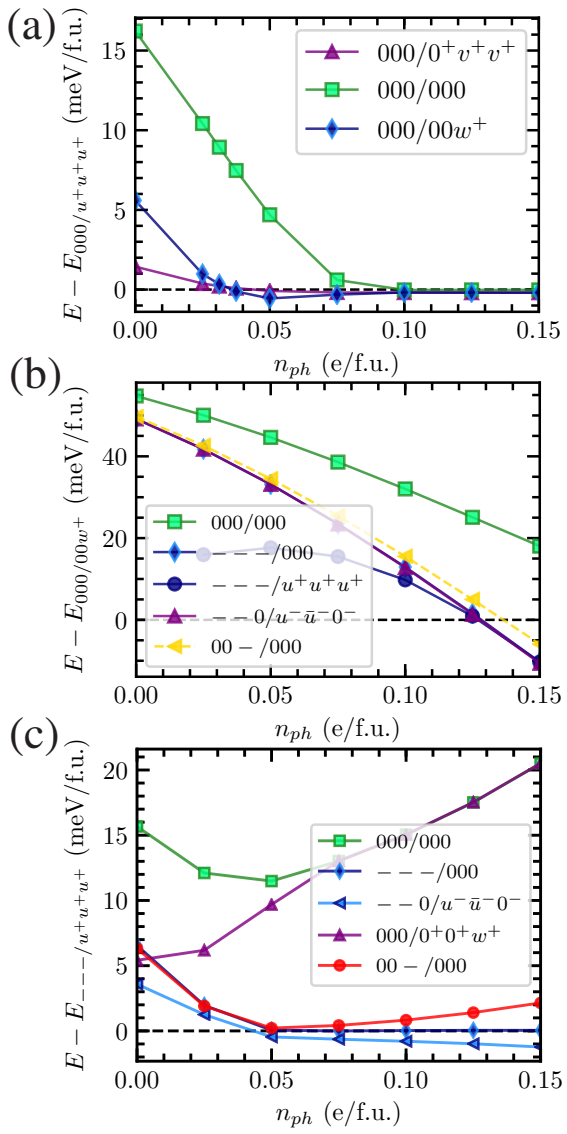

FIG. 3. (a) Energy of different phases in BTO with respect to the $000/u^+u^+u^+$ structure (dashed dark line), which is the ground state in the dark. The tetragonal $000/00w^+$ and then the cubic 000 phase become more energetically favorable. (b) Energy of different phases in PTO with respect to the $000/00w^+$ structure (dashed dark line), which is the ground state in the dark, showing that non-polar antiferrodistortive phases become more stable at large concentration of photo-excited carriers. (c) Energy of different phases in PSTO with respect to the rhombohedral $---/u^+u^+u^+$ structure (dashed dark line), which is the lowest energy phase considered when no carriers are excited.

material such as $SrTiO_3$, and form the solid solution $(Pb_{1/2}Sr_{1/2})TiO_3$ (PSTO) to favor the tilt instability with respect to the polar one. As a proof of concept, several phases of PSTO with rocksalt order were calculated in Fig. (3.c). In particular, a polar rhombohedral $---/u^+u^+u^+$ phase (black dashed line) is the ground state in the dark. The $000/00w^+$ (purple triangles) and the high-symmetry cubic 000/000 phase (in green squares) have increasing energy with n_{ph}. On the contrary, the antipolar tilted phase $--0/u^-\bar{u}^-0^-$ (light blue triangles) becomes the most stable phase above $n_{ph} = 0.05$ e/f.u., thus supporting the proposed design strategy to reduce the critical concentration for the polar-to-antipolar/antiferrodistortive transition.

From this work, it also becomes apparent that the ferroelectric instability can be hampered by the photogeneration of free carriers. Obviously, free carriers screen the long-range Coulombic interaction responsible for the polar order [37, 41], thus seemingly disfavoring polar phases with respect to non-polar ones. This is consistent with calculations [37, 41] and experiments [42] performed by doping BTO with free electrons. The former predicted the disappearance of the polar order in BTO at a concentration of extra-electrons of ≈ 0.1 e/f.u., which is exactly the concentration of photo-excited carriers that stabilizes the cubic phase in our calculations. We also note that the destruction of the polar order in BTO and the large stability (and metastability) window of the $000/00w^+$ phase in PTO are consistent with the doping calculations performed in Ref. [37]. In addition, photoexcitation tends to move electrons from O $2p$ states to Ti d states, thus destroying the covalent bonding that drives the ferroelectric order [40] and favoring non-polar orders. Looking at the evolution of interatomic force constants (IFCs; see Supplementary Material [31]) under photoexcitation, shows that *(i)* almost all IFCs are reduced in magnitude under photoexcitation, and *(ii)* the most affected IFCs corresponds to 4th nearest neighbors interaction, *i.e.* similar atoms (Ti-Ti, O-O, etc.) interacting along the $< 100 >$ cubic directions. This parallels the further stabilization of the paraelectric phase under photoexcitation in the incipient ferroelectric PbTe, which results from screening of the long-range Coulomb interactions by the redistributed photoexcited carriers along the $< 100 >$ cubic directions [38]. From the evidence presented here, as well as in other works involving doping and photoexcited calculations [37, 38], electrostatic screening by photoexcited carriers appears as a universal mechanism for "dipole-dipole driven" ferroelectric materials such as BTO [39].

In addition, the volume of most phases decreases with increasing concentration of excited carriers in both BTO and PTO, except that of the cubic 000/000 phase, which increases instead (see Supplementary Material [31]). Interestingly, the decrease of volume of the polar phases is consistent with the disappearance of the polar order, and is reminiscent of the well-known [17–19] effect of hydrostatic compression; yet, the volume increase of the cubic phase under illumination should in principle favor the polar instabilities. Hence, our results suggest that the behavior of the polar distortion upon illumination cannot be understood solely in terms of a photo-induced volume change [43], and that screening effects play a central role.

There are, however, potential limitations of this work,

since DFT is known to underestimate the quasi-particle bandgap. Furthermore, excitonic effects are described within a mean-field approximation using constrained DFT to mimic excited states occupations. First, we performed G_0W_0 [44] calculations with the Yambo [45] package - using DFT input from Quantum Espresso [46, 47] - in order to accurately describe the conduction and valence bands (see Supplementary Material [31]). The corrected band structure is overall not altered, except for an almost rigid upshift of the conduction bands. This shift slightly depends on the studied phase (with differences smaller than 100 meV between phases). The shift is smaller for non-polar phases, therefore facilitating further the light-induced transitions towards such latter states.

For BTO, we checked the robustness of our conclusions by performing calculations of zone center phonons of the cubic phase with hybrid DFT. We compare calculations performed with the semi-local PBEsol functional and the hybrid HSEsol [48] functional. Both functionals give similar lattice constants and similar frequency for the imaginary frequency of the soft ferroelectric mode, even though the band gaps are quite different (1.8 eV for PBEsol and 3.4 eV, close to the GW value, for HSEsol). Despite the very different band gaps, the phonon frequencies as a function of the excited charge density evolve similarly: we observe a stabilization of the soft mode at an excited charge density of 0.09 electron per formula unit (see Supplementary Material [31]). Hence, although our DFT-based description may slightly alter the critical concentrations at which transitions occur, the present qualitative behavior should be correct, especially given our results in Fig. 2 for the dynamical lattice instabilities of the *paraelectric cubic state*.

At last, let us discuss the possibility of having photo-induced phase transitions to (small self-trapped, or ST) polaronic states. Recent (doping) calculations have shown that ST holes were unlikely in PTO [49, 50], but could potentially be stabilized in cubic BTO [49]. In order to check the appearance of polaronic states, we ran calculations in BaTiO3 under photoexcitation with $n_{ph} = 0.075$ e/f.u. and $n_{ph} = 0.150$ e/f.u (with no symmetry). No trace of polaronic states was found.

In conclusion, we have shown that light absorption is a viable route to switch on/off specific lattice instabilities in complex materials such as ferroelectric perovskite oxides. Via first-principles calculations we have demonstrated the microscopic mechanism leading to a light-controlled stabilization of the cubic phase in BTO but not in PTO. The calculations are a promising tool to engineer and optimize such light-triggered transformations, suggesting strategies for their practical realization in suitably chosen materials. The results presented in this work could offer a route to design light-controlled memory, by accessing light-induced metastable states (see Fig. 4 in the Supplemental Material [31] and related discussion).

C. P. and L. B. thank the ARO grant W911NF-16-1-0227. We also acknowledge support from the National Research Fund, Luxembourg through project INTER/ANR/13/20/NANOTMD (E. T. and L. W.) and the intermobility program (Grant No. 15/9890527 Greenox, J. I. and L. B.). C. P. thanks the AHPCC and a DoD challenge grant for use of computing resources. We thank B. Dkhil and P. Ruello for interesting discussions.

* charles.paillard@centralesupelec.fr

[1] I. Grinberg, D. V. West, M. Torres, G. Gou, D. M. Stein, L. Wu, G. Chen, E. M. Gallo, A. R. Akbashev, P. K. Davies, J. E. Spannier, A. M. Rappe, *Nature* **503**, 509 (2013).
[2] B. I. Sturman, V. M. Fridkin, *The Photovoltaic and Photorefractive Effects in Noncentrosymmetric Materials*, Gordon and Breach Science Publishers (1992).
[3] L. Z. Tan, F. Zheng, S. M. Young, F. M. Wang, S. Liu, A. M. Rappe, *npj Computational Materials* **2**, 16026 (2016).
[4] C. Paillard, X. Bai, I. C. Infante, M. Guennou, G. Geneste, M. Alexe, J. Kreisel, B. Dkhil, *Advanced Materials* **28**, 5153 (2016).
[5] R. Nechache, C. Harnagea, S. Li, L. Cardenas, J. Chakrabartty, F. Rosei, *Nature Photonics* **9**, 61 (2014).
[6] B. Kundys, M., Viret, D., Colson, D. O. Kundys, *Nature Materials* **9**, 803 (2010).
[7] M. Lejman, G. Vaudel, I. C. Infante, P. Gemeiner, V. E. Gusev, B. Dkhil, P. Ruello,*Nat. Commun.* **5**, 4301 (2014).
[8] B. Kundys, *Applied Physics Reviews* **2**, 011301 (2015).
[9] Y. Cui, J., Briscoe, S. Dunn, *Chemistry of Materials* **25**, 4215 (2013).
[10] V. Iurchuk, D. Schick, J. Bran, D. Colson, A. Forget, D. Halley, A. Koc, M. Reinhardt, C. Kwamen, N. A. Morley, M. Bargheer, M. Viret, R. Gumeniuk, G. Schmerber, B. Doudin, B. Kundys, *Physical Review Letters* **117**, 107403 (2016).
[11] R. Guo, L. You, Y. Zhou, Z. S. Lim, X. Zou, L. Chen, R. Ramesh, J. Wang, *Nature Communications* **4**, 1990 (2013).
[12] Y.-H. Kuo, S. Nah, K. He, T. Hu, A. M. Lindenberg, *Journal of Material Chemistry C* **5**, 1522 (2017).
[13] A. M. Glazer, *Acta Crystallographica B* **28**, 3384 (1972).
[14] G. H. Kwei, A. C. Lawson, S. J. L. Billinge, S. W. Cheong, S. W. *The Journal of Physical Chemistry* **97**, 2368 (1993).
[15] G. Shirane, S. Hoshino, *Journal of the Physical Society of Japan* **6**, 265 (1951).
[16] P. Ghosez, E. Cockayne, U. V. Waghmare, K. M. Rabe, *Physical Review B* **60**, 836 (1999).
[17] I. A. Kornev, L. Bellaiche, P. Bouvier, P.-E. Janolin, B. Dkhil, J. Kreisel, *Physical Review Letters* **95**, 196804 (2005).
[18] P.-E. Janolin, P. Bouvier, J. Kreisel, P. A. Thomas, I. A. Kornev, L. Bellaiche, W. Crichton, M. Hanfland, B. Dkhil, *Physical Review Letters* **101**, 237601 (2008).
[19] M. Ahart, M. Somayazulu, R. E. Cohen, P. Ganesh, P. Dera, H.-k. Mao, R. J. Hemley, Y. Ren, P. Liermann & Z. Wu, *Nature* **451**, 545 (2008).
[20] H. Moriwake *et al.*, *J. Appl. Phys.* **119**, 064102 (2016).
[21] A. Kirilyuk, A. V. Kimel, T. Rasing, *Rev. Mod. Phys.*

82, 2731 (2010).

[22] A. Subedi, *Phys. Rev. B* **92**, 214303 (2015)

[23] X. Gonze *et al. Computational Physics Communications* **180**, 2582 (2009).

[24] P. E. Blöchl, *Physical Review B* **50**, 17953 (1994).

[25] M. Torrent, F. Jollet, F. Bottin, G. Zérah, X. Gonze, *Computational Material Science* **42**, 337 (2008).

[26] J. P. Perdew, A. Ruzsinszky, G. I. Csonka, O. A. Vydrov, G. E. Scuseria, L. A. Constantin, X. Zhou, K. Burke, *Physics Review Letters* **100**, 136406 (2008).

[27] W. Kohn, L. J. Sham, *Physical Review* **140**, A1133 (1965)

[28] J. P. Perdew, Y. Wang, *Physical Review B* **45**, 13244 (1992).

[29] P. Würfel, U. Würfel, *Physics of Solar Cells: From Basic Principles to Advanced Concepts*, Wiley-VCH (2009).

[30] A. Togo, I. Tanaka, *Scripta Materialia* **108**, 1 (2015).

[31] See Supplementary Material at ... for more details which includes Refs. [12, 14, 17–19, 37, 42, 43, 45–48, 51**? ?** –58]. We detail the symmetry and atomic displacement evolution under excitation of carriers; Nudge Elastic Band calculations show that the transition is likely to be first order and that the non-polar phase are not metastable, but rather unstable; we discuss the occurrence of a monoclinic phase in $BaTiO_3$; Volume changes under illumination are compared with hydrostatic pressure results from the literature. The evolution of Interatomic Force Constants is also depicted. Finally, via the GW-approximation and hybrid DFT calculations, we discuss the relevance of many-body effects for the photoiduced stabilization of the cubic phase.

[32] L. Belyaev, V. M. Fridkin, A. A. Grekov, N. A. Kosonogov, A. I. Rodin, *Le J. Phys. Colloq.* **33**, C2-123 (1972).

[33] Pump-probe experiments on $BiFeO_3$ in Ref. [7] estimate $n_{ph} \sim 5 \times 10^{19}$e cm^{-3} with maximum used fluences of $\sim 50\mu$J.cm^{-2}. In Ref. [12] (which observes a monoclinic phase in $BaTiO_3$ nanowires) fluences ranging up to 600μJ.cm^{-2} are used, which would correspond to a carrier concentration of $\sim \frac{600}{50}.5 \times 10^{19} \approx 6 \times 10^{20}$e cm^{-3}. This order of magnitude matches the region where we observed flattening of the energy landscape in Fig. 3a (around the $000/u^+u^+u^+$ to $000/00w^+$ transition) which could potentially harbor a monoclinic phase as discussed in the Supplementary Material [31].

[34] L. Bellaiche, J. Íñiguez, *Physical Review B* **88**, 014104 (2013).

[35] I. A. Kornev, L. Bellaiche, P.-E. Janolin, B. Dkhil, E. Suard *Physical Review Letters* **97**, 157601 (2006).

[36] J. C. Wojdeł, P. Hermet, M. P. Ljungberg, P. Ghosez, J. Íñiguez, *Journal of Physics: Condensed Matter* **25**, 305401 (2013).

[37] H. J. Zhao, A. Filippetti, C. Escorihuela-Sayalero, P. Delugas, E. Canadell, L. Bellaiche, V. Fiorentini, and J. Íñiguez, *Physical Review B* **97**, 054107 (2018).

[38] M.P. Jiang, M. Trigo, I. Savić, É. D. Murray, C. Bray, J. Clark, T. Henighan, M. Kozina, M. Chollet, J. M. Glownia, M. C. Hoffmann, D. Zhu, O. Delaire, A. F. May, B. C. Sales, A. M. Lindenberg, P. Zalden, T. Sato, R. Merlin, D. A. Reis, *Nat. Commun.* **7**, 12291 (2016).

[39] A. Filippetti, V. Fiorentini, F. Ricci, P. Delugas, J. Íñiguez, *Nat. Commun.* **7**, 11211 (2016).

[40] R. E. Cohen, *Nature* **358**, 136 (1992).

[41] Y. Wang, X. Liu, J. D. Burton, S. S. Jaswal, E. Y. Tsymbal, *Physical Review Letters* **109**, 247601 (2012).

[42] J. Fujioka *et al.*, *Scientific Reports* **5**, 13207 (2015).

[43] C. Paillard, S. Prosandeev, L. Bellaiche, *Physical Review B* **96**, 045205 (2017).

[44] M. S. Hybertsen, S. G. Louie, *Phys. Rev. B* **34**, 5390 (1986).

[45] Marini, A., Hogan, C., Grüning, M. & Varsano, D. Yambo: An ab initio tool for excited state calculations. *Comput. Phys. Commun.* **180**, 1392–1403 (2009).

[46] Giannozzi, P. *et al.* QUANTUM ESPRESSO: a modular and open-source software project for quantum simulations of materials. *J. Phys. Condens. Matter* **21**, 395502 (2009).

[47] Giannozzi, P. *et al.* Advanced capabilities for materials modelling with Quantum ESPRESSO. *J. Phys. Condens. Matter* **29**, 465901 (2017).

[48] L. Schimka, J. Harl, G. Kresse, *J. Chem. Phys.* **134**, 024116 (2011).

[49] P. Erhart, A. Klein, D. Åberg, B. Sadigh, *Phys. Rev. B* **90**, 035204 (2014).

[50] C. Paillard, G. Geneste, L. Bellaiche, B. Dkhil, *J. Phys. Condens. Matter* **29**, 485707 (2017).

[51] H. D. Megaw, *Acta Crystallographica* **5**, 739 (1952).

[52] E. Weinan, W. Ren, E. Vanden-Eijnden, *J. Chem. Phys.* **126**, 164103 (2007).

[53] Z.-G. Ye, B. Noheda, M. Dong, D. E. Cox, G. Shirane, *Physical Review B* **64**, 184114 (2001).

[54] L. Bellaiche, A. García, D. Vanderbilt, *Physical Review Letters* **84**, 5427 (2000).

[55] D. Sangalli, A. Ferretti, H. Miranda, C. Attaccalite, I. Marri, E. Cannuccia, P. Melo, M. Marsili, F. Paleari, A. Marrazzo, G. Prandini, P. Bonfà, M.O. Atambo, F. Affinito, M. Palummo, A. Molina-Sánchez, C. Hogan, M. Grüning, D. Varsano, A. Marini, arXiv:1902.03837 [cond-mat.mtrl-sci] (2019).

[56] C. Thomsen, H.T. Grahn, H.J. Maris, and J. Tauc, *Phys. Rev. B* **34**, 4129 (1986).

[57] R. Dovesi, A. Erba, R. Orlando, C. M. Zicovich-Wilson, B. Civalleri, L. Maschio, M. Rerat, S. Casassa, J. Baima, S. Salustro, B. Kirtman, *WIREs Comput Mol Sci.* **8**, e1360 (2018)

[58] G. Sophia, P. Baranek, C. Sarrazin, M. Rerat, R. Dovesi, *Phase Transitions: A Multinational Journal*, **81**, 1069-1084 (2013).